

Coherent elastic neutrino-nucleus scattering (CE ν NS) event rates for Ge, Zn, and Si detector materials

T. S. Kosmas,^{1,*} V. K. B. Kota,^{2,†} D. K. Papoulias^{1,‡} and R. Sahu^{3,§}

¹*Division of Theoretical Physics, University of Ioannina, GR 45110 Ioannina, Greece*

²*Physical Research Laboratory, Ahmedabad 380 009, India*

³*National Institute of Science and Technology, Palur Hills, Berhampur 761 008, Odisha, India*



(Received 23 August 2021; revised 16 November 2021; accepted 10 December 2021; published 30 December 2021)

Realistic nuclear structure calculations are presented for the event rates due to coherent elastic neutrino-nucleus scattering (CE ν NS), assuming neutrinos from pion decay at rest, from nuclear reactors, and from Earth's interior. We focus on the currently interesting germanium isotopes, ^{70,73,76}Ge, which constitute detector materials of the recently planned CE ν NS experiments. We study in addition the potential use of ^{64,70}Zn and ²⁸Si isotopes as promising CE ν NS detectors. From nuclear physics perspectives, recently, calculations have been carried out within the framework of the deformed shell model (DSM), based on realistic nuclear forces, and assessed on the reproducibility of spectroscopic nuclear properties. The high confidence level acquired by their agreement with experimental results and by their comparison with other mostly phenomenological calculations encouraged the use of DSM to extract predictions for the CE ν NS event rates of the above isotopes. Our detailed estimation of the nuclear physics aspects of the recently observed neutral current coherent neutrino-nucleus scattering may shed light on unravelling the still remaining uncertainties for the CE ν NS process within and beyond the standard model.

DOI: [10.1103/PhysRevC.104.064618](https://doi.org/10.1103/PhysRevC.104.064618)

I. INTRODUCTION

More than four decades ago, Freedman [1] proposed the measurement of the neutral current coherent elastic neutrino-nucleus scattering (CE ν NS) when low-energy neutrinos scatter off nuclei. This process, however, was observed for the first time very recently by the COHERENT Collaboration [2] using the sodium-doped CsI detector at the Spallation Neutron Source (SNS) at Oak Ridge National Laboratory. The process was, subsequently, observed at the SNS using also a liquid argon (LAr) detector [3]. The observation of CE ν NS has opened up new opportunities to test the predictions of the standard model (SM) [4–8], while a precise measurement of this process may offer a way to constrain the particle physics parameters of theories beyond the SM [9] (the recent constraints extracted from CE ν NS are summarized in Ref. [10]).

The detection signal of CE ν NS, i.e., the low-energy recoil of the target nucleus, is an experimental challenge while the uncertainties associated with the relevant measurements should be minimized and the accuracy of CE ν NS experimental method must be improved. Toward this purpose, many planned experiments for measuring CE ν NS are based on the well-known germanium detectors [11], while zinc and silicon are also promising detector materials for neutrino-nucleus cross-section measurements [12]. Such ongoing and designed

detectors are CONUS [13], ν GEN [14], TEXONO [15], COHERENT [16], RICOCHET [17], MINER [18], NUCLEUS [19], CONNIE [20], Coherent Captain-Mills (CCM) [21], European Spallation Source (ESS) [22], ν IOLETA [23], and SBC [24] experiments. The employment of pure Ge detectors in measuring rare event processes has shown appreciably good sensitivity, while in CE ν NS some combinations of detection media have been chosen and proposed to be utilized due to other experimental criteria [25]. Toward the latter purposes, Zn and Si isotopes may offer advantageous combinations to reduce the systematic errors of CE ν NS experiments instead of a single element [11].

Theoretically, it was known that roughly speaking the CE ν NS cross section has a quadratic dependence on the neutron number of the target nucleus ($\propto N^2$) which is attributed to the different strength of the respective couplings with which the protons and the neutrons of the atomic nuclei interact with the intermediate Z_0 boson; see, e.g., Ref. [26]. The ground-state to ground-state transition channel, which is possible in neutral current neutrino-nucleus scattering, appears enhanced due to the fact that the proton and neutron amplitude phases corresponding to a neutrino scattering off nucleons are added coherently [27] and dominate the process at low energies. On the other hand, the incoherent scattering cross sections are much smaller and demonstrate some well-pronounced peaks of specific multipole excitations [28]. Such detailed calculations have been performed previously for various nuclear isotopes (see, e.g., Refs. [29,30]).

With respect to physics beyond the SM, nonstandard interactions (NSIs) is a widely used formalism that can phenomenologically describe a large family of new physics

*hkosmas@uoi.gr

†vkbkota@prl.res.in

‡d.papoulias@uoi.gr

§rankasahu@gmail.com

interactions, in particular those involving novel vector or axial vector processes [31]. Constraints on NSIs exist from the analysis of available $\text{CE}\nu\text{NS}$ data by COHERENT with CsI [9,33,34] and LAr [35]. Moreover, extensions of the NSI formalism, namely neutrino generalized interactions (NGIs) can accommodate scalar, pseudoscalar, and tensor interactions [32].

Over the years, the deformed shell model (DSM) based on Hartree-Fock (HF) states with angular momentum projection and band mixing has been found to be quite successful in describing several nuclear properties like spectroscopic properties including spectroscopy of $N = Z$ odd-odd nuclei with isospin projection [36], the coherent and incoherent neutral current $\mu \rightarrow e$ conversion in the field of nuclei [37], and double- β decay half-lives [38,39]. Recently, we have calculated event rates for weakly interacting massive particle (WIMP) scattering off ^{73}Ge [40] and elastic and inelastic scattering of neutrinos and WIMPs on nuclei [6,41]. Our aim in this work is to provide reliable theoretical predictions for event rates of neutrino-nucleus scattering involving $^{70,73,76}\text{Ge}$, $^{64,70}\text{Zn}$, and ^{28}Si isotopes by using DSM for the nuclear structure functions needed for the event rate calculations. Motivated by the various experimental facilities, first, we focus on pion decay at rest (π -DAR) and reactor antineutrino sources. We furthermore consider geoneutrinos, which are expected to contribute sizable the overall neutrino background signal at the next-generation large-scale detectors planned to look for light WIMPs [42].

Finally, we quantify the percentage differences on the expected number of events obtained with the DSM, as compared to those relying on the widely used approximate form factor parametrizations, at different energy regimes, as well as to those obtained with different nuclear physics methods [43]. We stress that, in extracting the percentage differences we rely on the number of events of the $\text{CE}\nu\text{NS}$ which is the most relevant experimental observable.

The paper has been organized as follows: In Sec. II, we discuss the $\text{CE}\nu\text{NS}$ formalism and our adopted nuclear structure method calculated in the framework of the DSM. Then, in Sec. III, we present the theoretical event rates and we discuss the level of inconsistency with respect to similar calculations involving effective nuclear form factors. Finally, our conclusions are summarized in Sec. IV.

II. BASIC FORMALISM

In this section, we present the basic formalism for calculating the $\text{CE}\nu\text{NS}$ event rates at different facilities aiming to detect signals induced by π -DAR, reactor, or geoneutrinos. We pay special attention to discussing the key ingredients of the nuclear physics aspects that have been taken into consideration. In particular, the nuclear form factors are obtained using nuclear wave functions determined by DSM, of which the confidence level is well established through the reproducibility of spectroscopic results for the nuclear isotopes of interest (see below).

Before embarking to the nuclear physics calculations, it is worth mentioning that, interesting studies of physics beyond the standard model include deviations from unitarity

[44], sterile neutrinos [44–46], neutrino magnetic moments [47–49], nonstandard interactions [32,34,50,51], light new physics [31,52], dark matter [53,54], etc.

A. $\text{CE}\nu\text{NS}$ differential cross section

Neutrinos with energies below some tens of MeV predominately conserve the integrity of nucleons in neutrino-quark interactions with Z_0 -boson exchange, allowing us to consider the $\text{CE}\nu\text{NS}$ process using an effective neutrino nucleon interaction in which the nucleon current is a sum of vector and axial currents. The differential $\text{CE}\nu\text{NS}$ cross section with respect to the nuclear recoil energy T_A (the axial vector contributions is neglected in this work) reads [9]

$$\frac{d\sigma}{dT_A} = \frac{G_F^2 m_A}{2\pi} Q_W^2 \left(2 - \frac{m_A T_A}{E_\nu^2} \right), \quad (1)$$

where G_F is the Fermi's constant, E_ν is the incoming neutrino energy, while Z and $N = A - Z$ denote the number of protons and neutrons, respectively. The vector weak charge, Q_W , encapsulates the information from the nuclear structure and is written in terms of the proton and neutron form factors $F_{p,n}(q^2)$ as

$$Q_W = g_p^V Z F_p(q^2) + g_n^V N F_n(q^2), \quad (2)$$

where the proton and neutron couplings are expressed as $g_p^V = 1/2 - 2 \sin^2 \theta_W$ and $g_n^V = -1/2$, respectively, and $q = \sqrt{2m_A T_A}$ denotes the magnitude of the 3-momentum transfer. For the low energies involved in $\text{CE}\nu\text{NS}$, our calculations consider the low-energy limit of the weak mixing angle running, and hence we assume $\sin^2 \theta_W = 0.2381$ [55]. Note that due to the smallness of the proton coupling, the $\text{CE}\nu\text{NS}$ cross section scales with a characteristic N^2 dependence. Finally, the nuclear mass is calculated as $m_A = Zm_p + Nm_n - B$, where the nuclear binding energy B is taken from Ref. [56] (the nucleon masses are taken to be $m_p = 938.28$ MeV and $m_n = 939.57$ MeV).

B. $\text{CE}\nu\text{NS}$ event rates

The differential and integrated event rates of $\text{CE}\nu\text{NS}$ after defining all the parameters in Eq. (1) are calculated by

$$\frac{dR}{dT_A} = \mathcal{K} \int_{E_{\nu,\min}}^{E_{\nu,\max}} \left[\frac{d\sigma}{dT_A}(E_\nu, T_A) \right] \lambda_\nu(E_\nu) dE_\nu, \quad (3)$$

where $\lambda_\nu(E_\nu)$ represents the relevant neutrino energy distribution function characterizing the specific neutrino source. The normalization factor \mathcal{K} is given by $\mathcal{K} = t_{\text{run}} \Phi_\nu N_{\text{targ}}$, with $N_{\text{targ}} = \frac{m_{\text{det}} N_A}{M_r}$. Here, t_{run} is taken as 1 yr, N_{targ} is the number of target nuclei, and Φ_ν is the neutrino flux normalization. In the calculation of N_{targ} , the detector mass m_{det} is assumed to be 1 kg for π -DAR and reactor neutrinos and 1 ton for geoneutrinos. Similarly, M_r is the molar mass (atomic weight) and N_A is the Avogadro number ($N_A = 6.022 \times 10^{23}$) [4].

For the case of π -DAR neutrinos, we consider the specifications of the SNS at Oak Ridge with $r = 0.08$ being the number of emitted neutrinos per flavor for each proton on target (POT) and $N_{\text{POT}} \approx 2.1 \times 10^{23}$ denoting the number of

protons on target per year [2]. The SNS flux is then obtained as $\Phi_\nu = \frac{r \cdot N_{\text{POT}}}{4\pi L^2}$, which for a typical detector baseline of $L \approx 20$ m, evaluates to $\Phi_\nu \approx 1 \times 10^7 \text{ s}^{-1} \text{ cm}^{-2}$. Finally, the neutrino energy distribution functions $\lambda_\nu(E_\nu)$ for SNS neutrinos are [57]

$$\lambda_\nu(E_\nu) = \begin{cases} \delta(E_\nu - \frac{m_\pi^2 - m_\mu^2}{2m_\pi}) & \text{prompt } \nu_\mu, \\ \frac{64E_\nu^2}{m_\pi^3} (\frac{3}{4} - \frac{E_\nu}{m_\mu}) & \text{delayed } \nu_e, \\ \frac{192E_\nu^2}{m_\pi^3}, (\frac{1}{2} - \frac{E_\nu}{m_\mu}) & \text{delayed } \bar{\nu}_\mu. \end{cases} \quad (4)$$

In the present work, the reactor antineutrino energy distribution which assumes the fission products of ^{235}U , ^{238}U , ^{239}Pu , and ^{241}Pu is taken from Ref. [58]. We note that, due to the lack of experimental data for $E_\nu < 2$ MeV, the theoretical calculation of Ref. [59] is employed, while we assume a typical flux of $\Phi_\nu \approx 1 \times 10^{13} \text{ s}^{-1} \text{ cm}^{-2}$. Similarly, for the case of geoneutrinos, the corresponding antineutrino energy distributions for the K, Th, and U chains are taken from Ref. [60]. It is worth noting that presently the flux uncertainties are quite large due to low statistics [61] while the geoneutrino flux depends largely on the location [42]. Here, we comply with the normalizations quoted in Ref. [62], which correspond to the location of the LNGS (Gran Sasso National Laboratory).

The differential number of events is obtained through the convolution of the differential cross section with the neutrino energy distribution $\lambda_\nu(E_\nu)$. The lower integration limit in Eq. (3) is trivially obtained from the CE ν NS kinematics and reads

$$E_{\nu,\text{min}} = \frac{1}{2}(T_A + \sqrt{T_A^2 + 2m_A T_A}) \approx \sqrt{\frac{m_A T_A}{2}}. \quad (5)$$

Note that $E_{\nu,\text{max}} = m_\mu/2 = 52.8$ MeV for the case of π -DAR neutrinos, while $E_{\nu,\text{max}} \approx 9.5$ MeV for reactor neutrinos and $E_{\nu,\text{max}} \approx (1.3, 2.3, 4.5)$ MeV for the (K, Th, U) geoneutrinos, respectively.

Finally, an additional integration over the nuclear recoil energy T_A , from a threshold energy T_A^{thres} up to a maximum energy $T_A^{\text{max}} = \frac{2E_{\nu,\text{max}}^2}{2E_{\nu,\text{max}} + m_A} \approx \frac{2E_{\nu,\text{max}}^2}{m_A}$, needs to be performed in order to obtain the expected number of events.

C. Deformed shell model

The details of the deformed shell model have been described in our earlier publications (for details see Ref. [63]). In this model, for a given nucleus, starting with a model space consisting of a given set of spherical single-particle (sp) orbitals with single-particle energies (spe) and an effective two-body interaction specified by its two-body matrix elements (TBME), the lowest energy intrinsic states are obtained by solving the HF single-particle equation self-consistently. We assume axial symmetry, while excited intrinsic configurations are obtained by making particle-hole excitations over the lowest intrinsic state. Since the intrinsic states denoted by $\chi_K(\eta)$ do not have definite angular momenta, states of good angular momentum are projected from the latter, which can

be written in the form

$$|\psi_{MK}^J(\eta)\rangle = \frac{2J+1}{8\pi^2\sqrt{N_{JK}}} \int d\Omega D_{MK}^*(\Omega) R(\Omega) |\chi_K(\eta)\rangle, \quad (6)$$

where N_{JK} is the normalization constant given by

$$N_{JK} = \frac{2J+1}{2} \int_0^\pi d\beta \sin\beta d_{KK}^J(\beta) \langle \chi_K(\eta) | e^{-i\beta J_y} | \chi_K(\eta) \rangle. \quad (7)$$

In Eq. (6), Ω represents the Euler angles (α, β, γ) , and $R(\Omega) = \exp(-i\alpha J_z) \exp(-i\beta J_y) \exp(-i\gamma J_z)$ represents the general rotation operator. However, it is worth noting that the good angular momentum states, projected from different intrinsic states, are not in general orthogonal to each other. Hence, they are orthonormalized and then band mixing calculations are performed. The resulting eigenfunctions are of the form

$$|\Phi_M^J(\eta)\rangle = \sum_{K,\alpha} S_{K\eta}^J(\alpha) |\psi_{MK}^J(\alpha)\rangle, \quad (8)$$

with $S_{K\eta}^J(\alpha)$ being the expansion coefficients. The nuclear matrix elements occurring in the calculation of event rates are evaluated using the wave functions $|\Phi_M^J(\eta)\rangle$. We finally stress that the DSM is well established enough to be a successful model for transitional nuclei with $A = 60\text{--}90$ [63], while recently it has also been used successfully for heavier nuclei like ^{127}I , ^{133}Cs , and ^{133}Xe [6].

III. RESULTS FOR CE ν NS EVENT RATES

The nuclei selected in the present study, $^{70,73,76}\text{Ge}$, $^{64,70}\text{Zn}$, and ^{28}Si , are of current experimental interest and therefore calculations for CE ν NS event rates that take into account the details of the nuclear structure are important. Firstly, the Ge isotopes are discussed in Ref. [25] with the most relevant experiments being the COHERENT [2,3], the CONUS [27,64], ν GEN [14], and the TEXONO [47], which use ionization-based Ge-semiconductors. Similarly, the (Si, Zn, Ge) isotopes have been chosen as the detector materials of the MINER [18], NUCLEUS [19], and RICOCHET [17], which employ cryogenic detectors.

We should, moreover, add that high-purity germanium (HPGe) detectors are used, for example, in CONUS experiment where the detector is located at 17.1 m from the reactor core (4 detectors each with ≈ 1 kg) and the expected $\bar{\nu}_e$ flux is $2.3 \times 10^{13} \text{ s}^{-1} \text{ cm}^{-2}$; see, e.g., Ref. [64]. Also, for the Chooz experiment Ge-based and metallic Zn-based detectors of mass

TABLE I. Nuclear structure properties of the studied isotopes (for details regarding the model space chosen, the sp energies, etc., see the text).

Nucleus	Germanium			Zinc		Silicon
	^{70}Ge	^{73}Ge	^{76}Ge	^{64}Zn	^{70}Zn	^{28}Si
Property						
Ground state spin (J^π)	0 ⁺	9/2 ⁺	0 ⁺	0 ⁺	0 ⁺	0 ⁺
Isotopic abundance (%)	20.52	7.76	7.75	49.2	0.6	92.2
H.o. length (fm)	1.894	1.907	1.920	1.865	1.894	1.625

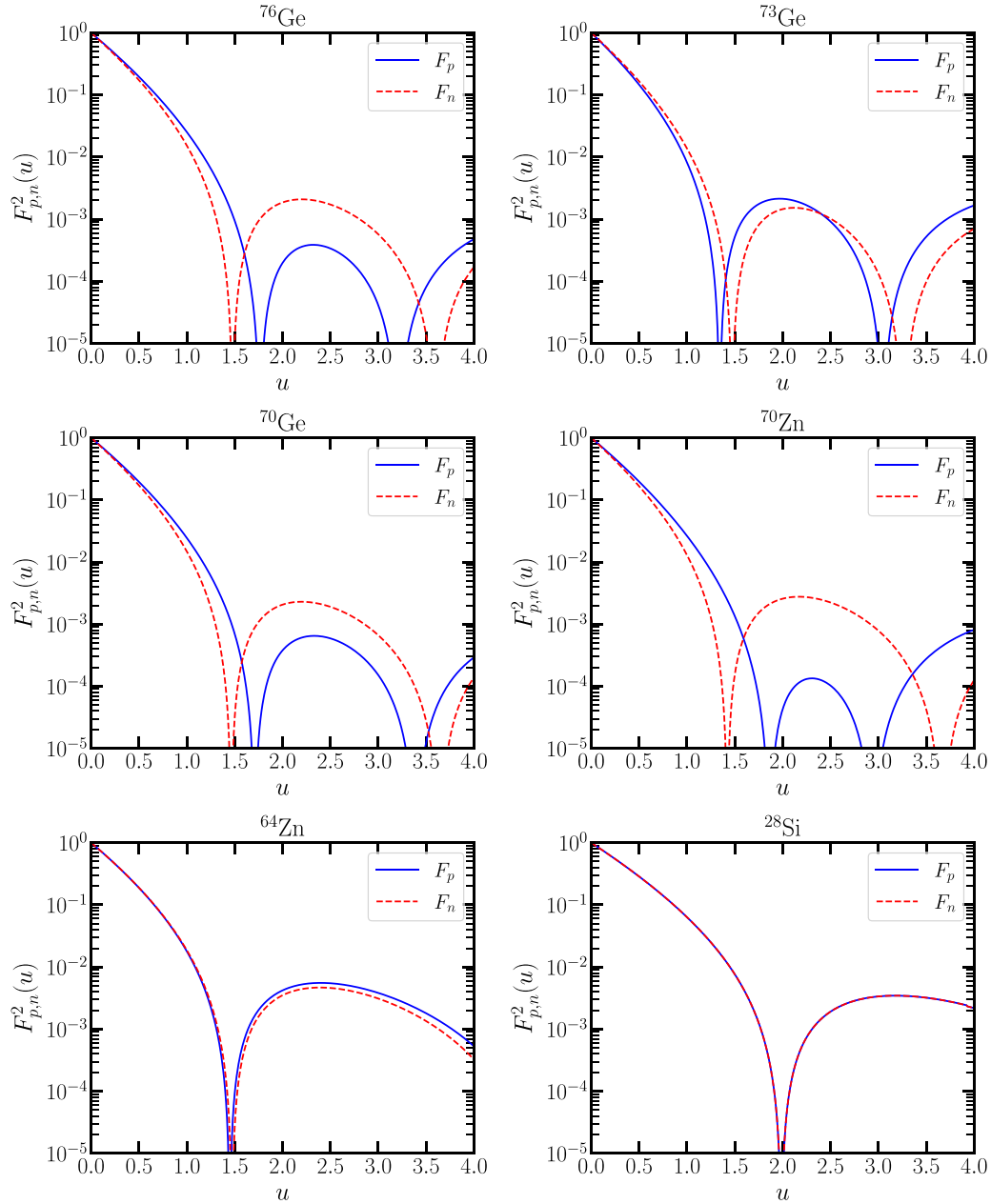


FIG. 1. Square of proton (solid line) and neutron (dotted line) form factors for $^{70,73,76}\text{Ge}$, $^{64,70}\text{Zn}$, and ^{28}Si as a function of $u = q^2 b_\ell^2/2$.

$m_{\text{det}} \approx 10$ kg are under deployment, with a reported threshold as low as 100 eV [17].

A. Nuclear structure calculations within the DSM

As is well known, the largest source of theoretical uncertainty in $\text{CE}\nu\text{NS}$ originates from the nuclear physics [5] (see also Ref. [4]). In this subsection, we evaluate the corresponding nuclear form factors with high reliability by incorporating our realistic nuclear structure DSM calculations. In Table I, some useful nuclear structure properties of the isotopes studied in the present work are tabulated. In the following paragraphs, for the benefit of the reader we describe briefly some basic properties of the studied $\text{CE}\nu\text{NS}$ detector materials.

1. The studied isotopes as $\text{CE}\nu\text{NS}$ detectors

- (1) For the ^{70}Ge isotope, in our earlier double- β decay (DBD) study using DSM [39], calculations have been carried out for spectroscopic properties such as the energy spectra (band structures), the $B(E2)$ values and occupancies. For this isotope, the $jj44b$ effective interaction in a model space consisted of the $^2p_{3/2}$, $^1f_{5/2}$, $^2p_{1/2}$, $^1g_{9/2}$ j levels with single particle (sp) energies (-9.6566 , -9.2859 , -8.2695 , -5.8944) MeV respectively [65], gave good agreement with data. Additional isotopic properties are listed in Table I. We note that for the harmonic oscillator (h.o.) size (length) parameter we used the simple expression $b_\ell = 0.933 A^{1/6} = 1.894$ fm for all the nuclei studied.

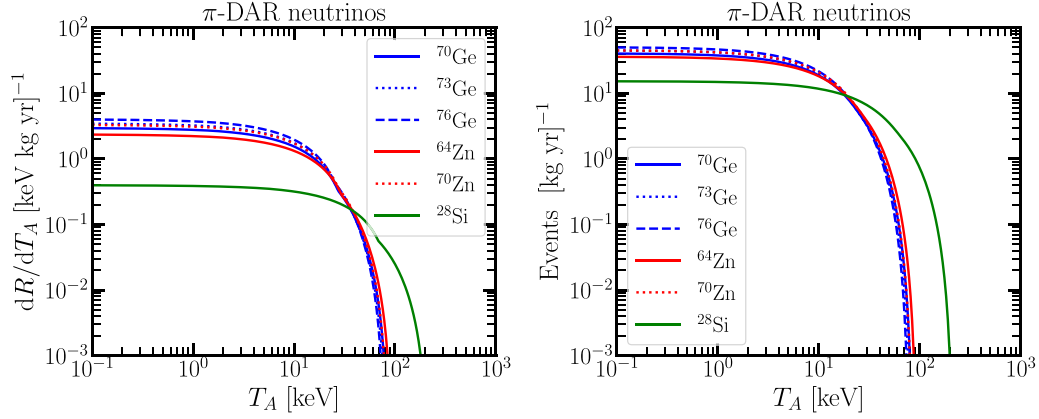


FIG. 2. Differential (left) and integrated (right) event rates as a function of the nuclear recoil energy for $^{70,73,76}\text{Ge}$, $^{64,70}\text{Zn}$, and ^{28}Si . The results are presented for CE ν NS process with π -DAR neutrinos.

- (2) For the ^{73}Ge , the DSM calculations have been assessed through the spectroscopic properties in Ref. [40] by employing the modified Kuo effective interaction [66] in the model space $^2p_{3/2}$, $^1f_{5/2}$, $^2p_{1/2}$, $^1g_{9/2}$, with the sp energies (0, 0.78, 1.08, 4.9) MeV, respectively. Band structures and other spectroscopic properties are well reproduced with the aforementioned ingredients. We also mention that in our recent CE ν NS results for ^{73}Ge in Ref. [6] we have adopted the same model parameter values with $b_\ell = 1.907$ fm.
- (3) For the ^{76}Ge isotope, which is a well-known neutrinoless double- β decay (DBD) detector material, the DSM calculations have been performed with the modified Kuo interaction and the same model space as well as sp energies as in the case of the ^{73}Ge isotope above ($b_\ell = 1.920$ fm) [38]. Low-lying bands, $B(E2)$ values, and orbit occupancies are well reproduced for this isotope too.
- (4) The DSM calculations for the ^{64}Zn isotope have been carried out using GXPF1A effective interaction [38]. The model space consisted of the $(^1f_{7/2}, ^2p_{3/2}, ^1f_{5/2}, ^2p_{1/2})$ orbits with sp energies $(-8.6240, -5.6793, -1.3829, -4.1370)$ MeV, respectively [67]. The en-

ergy spectra, the $B(E2)$ values, and occupancies of sp orbits (with $b_\ell = 1.865$ fm) agree very well with the corresponding experimental data [38].

- (5) For ^{70}Zn , the DSM spectroscopic results have been obtained with the ingredients of ^{70}Ge as described above ($b_\ell = 1.894$) [39].
- (6) For the ^{28}Si , the spectroscopic calculations within DSM have been performed ($b_\ell = 1.625$ fm) by using the recently determined USD effective interaction [68,69]. The calculated energy spectra, the $B(E2)$'s, and also the $B(M1)$ values agree reasonably well with the experimental data and they will be discussed elsewhere [70].

Although we have used a formula for b_ℓ following the DSM study of ^{72}Ge in Ref. [37], it is desirable to deduce the values of b_ℓ for each isotope from proton charge radii obtained by electron scattering experiments. The experimental values for the charge radii (in fm) are 4.041, 4.063, 4.081, 3.928, 3.985, and 3.122 for $^{70,73,76}\text{Ge}$, $^{64,70}\text{Zn}$, and ^{28}Si as given in Ref. [71]. However, theoretical calculations for charge radii (see Ref. [72] for shell model and Ref. [73] for HFB examples) involve not only b_ℓ as a parameter but also effective charges. A consistent analysis of experimental data for charge

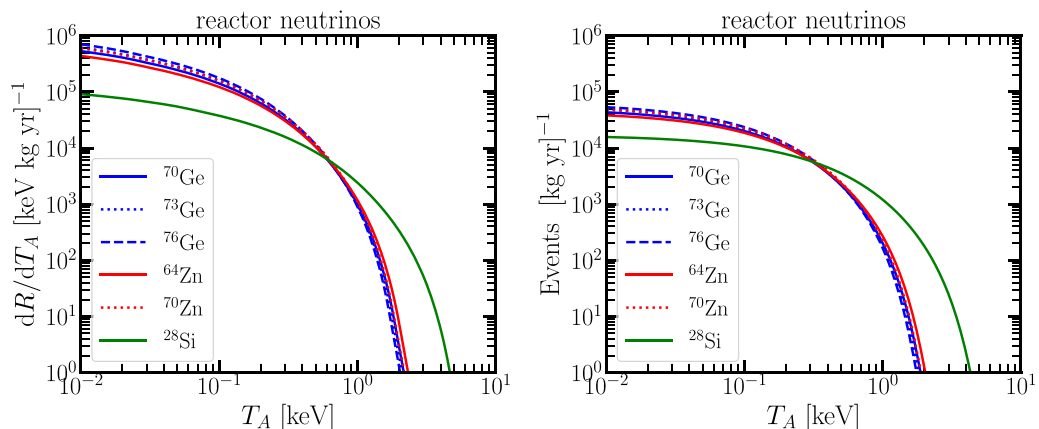


FIG. 3. Differential (left) and integrated (right) event rates as a function of the nuclear recoil energy for $^{70,73,76}\text{Ge}$, $^{64,70}\text{Zn}$, and ^{28}Si . The results are presented for CE ν NS process with reactor neutrinos.

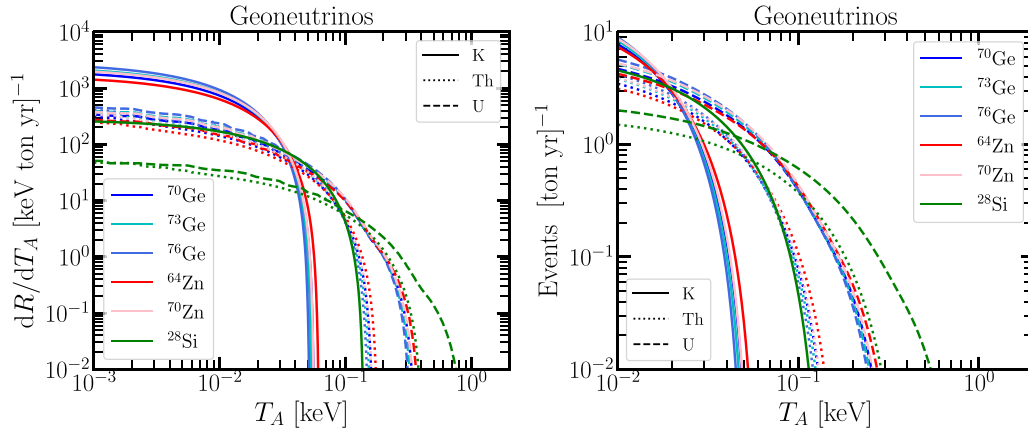


FIG. 4. Differential (left) and integrated (right) event rates as a function of the nuclear recoil energy for $^{70,73,76}\text{Ge}$, $^{64,70}\text{Zn}$, and ^{28}Si . The results are presented for $\text{CE}\nu\text{NS}$ process with reactor neutrinos.

form factors, charge radii, quadrupole moments, and $B(E2)$ values using DSM for the nuclei studied here will be considered in a future work. Finally, we note that the length parameter $b_\ell = 0.933 A^{1/6}$ (in fm) used (see Table I) is slightly smaller than the conventional parametrization $\hbar\omega = 41 A^{1/3}$ giving $b_\ell = 0.994 A^{1/6}$.

B. DSM calculations of the nuclear form factors needed for $\text{CE}\nu\text{NS}$ event rates

The proton and neutron nuclear form factors, $F_{p,n}(u)$, in terms of the dimensionless parameter $u = q^2(b_\ell)^2/2$, are illustrated in Fig. 1. As can be seen from this figure, for the even-even isotopes ^{76}Ge , ^{70}Ge , and ^{70}Zn , the neutron form factor peaks shift toward smaller values of u . Again, the second neutron peak is larger than the corresponding proton peak. For the other three nuclear isotopes, the neutron and proton form factors are almost similar. Further details for the nuclei of interest, on the chosen nuclear configuration, the effective interaction, the b_ℓ value, etc., are listed in Table I and are discussed previously.

By employing the form factors shown in Fig. 1, the differential and integrated event rates are calculated utilizing Eq. (3) for neutrinos of the SNS, reactor, and geoneutrino sources and the results are illustrated in Figs. 2–4. In these plots, we have used different isotopes of the same element, which is crucial for reducing the systematic errors as pointed out in Ref. [25]. For example, for SNS the proportion of differential event rates for $^{70,73,76}\text{Ge}$ at recoil energy 0.1 keV is 2.96:3.64:4.0, which is equivalent to 1:1.230:1.351.

Assuming that the N^2 dependence is approximately valid, the corresponding proportions are $38^2:41^2:44^2$, which is equivalent to 1:1.164:1.340. For the case of reactor neutrons, the corresponding proportions are 1:1.213:1.316. For other cases also, we obtain similar results. Use of detectors made up of a set of isotopes of an element may help in precision measurements at different experimental facilities.

Turning to large-scale dark matter direct detection detectors, our current results indicate sizable geoneutrino-induced event rates, especially for sub-keV thresholds. Even though the detectable geoneutrino background signal will be com-

pletely dominated by solar neutrino events, it is expected to become a crucial component in the overall neutrino background at future ton-scale detectors looking for WIMPs, especially for those aiming to detect low-mass WIMPs with $m_\chi \leq 10 \text{ GeV}/c^2$. As a concrete example, we discuss the SuperCDMS experiment at SNOLAB which aims to reach nuclear recoil thresholds as low as 40 eV (78 eV) using a germanium (silicon) detector [74] for which our present calculations are particularly relevant and of significant importance.

Finally, we are interested to quantify the percentage difference on the number of events calculated using our nuclear structure DSM calculations or involving effective form factor approximations. As a benchmark test case, we consider the Klein-Nystrand form factor approximation [75] that has been recently adopted by the COHERENT Collaboration [2]. We illustrate the difference between the two calculations by evaluating the quantity

$$\mathcal{R} = \frac{|R_{\text{DSM}} - R_{\text{KN}}|}{R_{\text{DSM}}} \quad (9)$$

and our corresponding results are shown in Fig. 5. As can be seen, reactor neutrino experiments looking for $\text{CE}\nu\text{NS}$ will not suffer from nuclear structure uncertainties, even at the sub-percentage level. On the other hand, for the case of π -DAR neutrinos which involve larger values of the momentum transfer, \mathcal{R} can be as high as 8% for ^{64}Zn and ^{76}Ge . We finally note that here we do not present the corresponding results for geoneutrinos since the signal uncertainty will be dominated by the flux uncertainties, while also the momentum transfer is lower compared to reactor neutrinos. For solar, diffused supernova background, and atmospheric neutrinos, such results have been presented in a previous study [41].

C. Application to nonstandard interactions

Focusing on vector-type NSIs only, our goal is to explore the impact of DSM form factors to the projected NSI sensitivities. In order to quantify the effect of nonzero NSI contributions to the $\text{CE}\nu\text{NS}$ cross section, it is sufficient to replace the SM weak charge of Eq. (2) with the corresponding

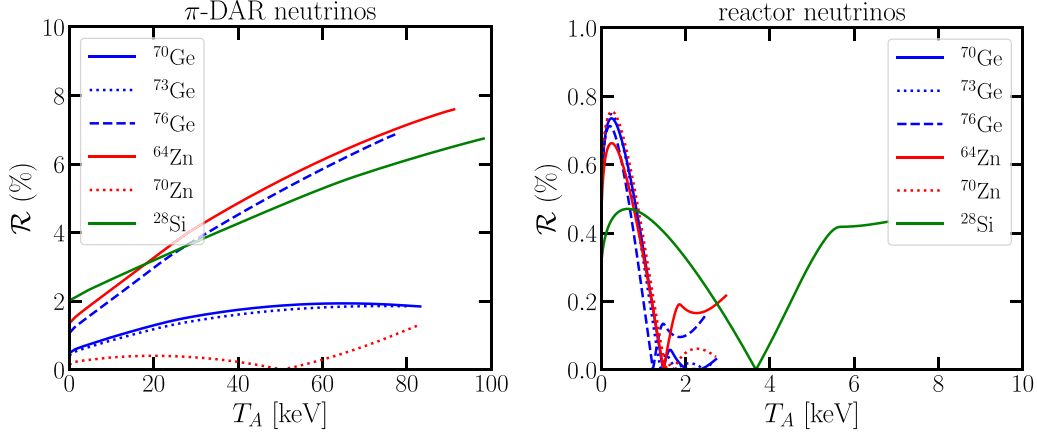


FIG. 5. Percentage difference between DSM calculations and those involving the effective Klein-Nystrand form factor parametrization (for details see the text). The results are presented for the case of π -DAR neutrinos (left) and reactor neutrinos (right) as a function of the nuclear recoil energy for $^{70,73,76}\text{Ge}$, $^{64,70}\text{Zn}$, and ^{28}Si .

NSI charge according to the substitution $Q_W \rightarrow Q_{\text{NSI}}$, with

$$\begin{aligned} Q_{\text{NSI}}^V = & [(g_V^p + 2\varepsilon_{\alpha\alpha}^{uV} + \varepsilon_{\alpha\alpha}^{dV})ZF_p(Q^2) \\ & + (g_V^n + \varepsilon_{\alpha\alpha}^{uV} + 2\varepsilon_{\alpha\alpha}^{dV})NF_n(Q^2)] \\ & + \sum_{\alpha} [(2\varepsilon_{\alpha\beta}^{uV} + \varepsilon_{\alpha\beta}^{dV})ZF_p(Q^2) \\ & + (\varepsilon_{\alpha\beta}^{uV} + 2\varepsilon_{\alpha\beta}^{dV})NF_n(Q^2)]. \end{aligned}$$

Our sensitivity analysis is based on a simple χ^2 function,

$$\chi^2 = \sum_{i=1}^{50} \left(\frac{R_{\text{SM}}^i - (1+a)R_{\text{NSI}}^i(\varepsilon_{ee}^{uV}, \varepsilon_{ee}^{dV})}{\sigma_{\text{stat}}^i} \right)^2 + \left(\frac{a}{\sigma_a} \right)^2, \quad (10)$$

for which we consider 50 equal-size bins of recoil energy in the range 5–80 keV, allowing for nonzero NSIs with the ν_e flux only. The statistical uncertainty is defined as $\sigma_{\text{stat}}^i = \sqrt{R_{\text{SM}}^i + R_{\text{bkg}}^i}$, assuming a flat background $R_{\text{bkg}}^i = \sigma_{\text{bkg}} R_{\text{SM}}^i$. We furthermore consider a conservative scenario taking the

background and signal uncertainties to be $\sigma_{\text{bkg}} = \sigma_a = 30\%$. For our statistical analysis, we assume a π -DAR neutrino source with a 10-kg ^{76}Ge target nucleus for which we expect the impact of nuclear form factors to be maximized (see left panel of Fig. 5).

Taking one nonvanishing NSI parameter at a time, our results are presented in Fig. 6. As can be seen from the χ^2 profiles, the use of DSM or KN form factors will not alter the sensitivities on ε_{ee}^{uV} . On the other hand, for the case of ε_{ee}^{dV} our fit clearly prefers the trivial solution over the nonzero one when relying on DSM nuclear structure calculations. This is found to be in contrast to the case of KN calculations where there is absence of a best-fit point preference. A few comments are in order. As expected, the sensitivity on ε_{ee}^{dV} is stronger compared to ε_{ee}^{uV} , and hence the implications of DSM calculations are more pronounced in the former case, which might be helpful for resolving the LMA dark degeneracy [76]. As a final remark, we have checked that the neutrino-floor explored in Ref. [77], due to the currently large uncertainties, is not affected by the choice of phenomenological or nuclear structure form factors.

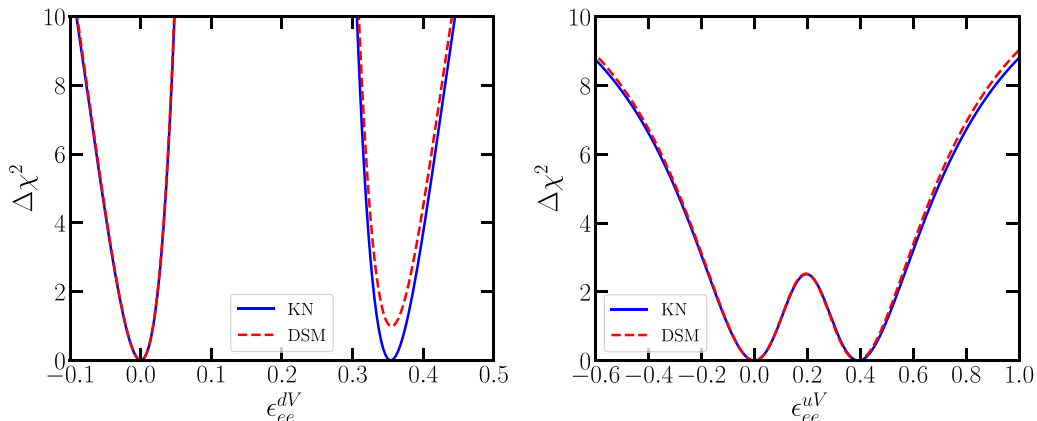


FIG. 6. Projected sensitivity to NSIs for a 10-kg ^{76}Ge detector at a π -DAR facility. A comparison of the expected sensitivities is given assuming DSM and KN nuclear form factors.

IV. CONCLUSIONS

Our main aim in the present study was to perform calculations of the $CE\nu NS$ event rates for the Ge detectors chosen in ongoing and designed $CE\nu NS$ experiments. We also studied Zn and Si, which are considered promising target materials of experiments aiming to measure $CE\nu NS$ events. The nuclear structure calculations have been carried out (for the specific isotopes $^{70,73,76}\text{Ge}$, $^{64,70}\text{Zn}$ and ^{21}Si) with a high level of reliability, by taking into account crucial information from the nuclear structure. The detailed nuclear physics aspects came out of the DSM method which involves realistic two-body interactions and is assessed on the reproducibility of experimental microscopic nuclear properties.

Highly accurate calculations, such as those provided here, are valuable for discriminating the expected signal from the various isotopic admixtures contained in germanium or zinc detectors, the use of which has been proposed for reducing the experimental uncertainties. We have considered typical experimental configurations, exposed to neutrinos from π -DAR, reactor antineutrinos, and geoneutrinos, while to the best of our knowledge, the present work is the first nuclear-physics-based study with regards to geoneutrino signals.

We compared our theoretical event rates with those calculated on the basis of the widely adopted form factors (e.g.,

the phenomenological Klein-Nystrand) and we concluded that especially for the SNS neutrinos the differences can be of the order of 10%. On the other hand, we have verified that reactor antineutrino facilities with sub-keV thresholds as well as large-scale direct dark matter detection experiments looking for light WIMPs uncertainties may be neglected for very low momentum transfer involved in the $CE\nu NS$ process. We have finally discussed the robustness of the attainable sensitivities on NSI with regards to phenomenological and DSM nuclear form factors.

ACKNOWLEDGMENTS

The research of D.K.P. is cofinanced by Greece and the European Union (European Social Fund, ESF) through the operational program “Human Resources Development, Education and Lifelong Learning” in the context of the project “Reinforcement of Postdoctoral Researchers, 2nd Cycle” (MIS-5033021), implemented by the State Scholarships Foundation (IKY). R.S. is thankful to SERB of Department of Science and Technology (Government of India) for financial support. The work of T.S.K. is implemented through the operational program “Human Resources Development, Education and Lifelong Learning, cycle B” (MIS-5047635) and is cofinanced by the European Union (European Social Fund) and Greek national funds.

-
- [1] D. Z. Freedman, Coherent neutrino nucleus scattering as a probe of the weak neutral current, *Phys. Rev. D* **9**, 1389 (1974).
 - [2] D. Akimov *et al.* (COHERENT Collaboration), Observation of coherent elastic neutrino-nucleus scattering, *Science* **357**, 1123 (2017).
 - [3] D. Akimov *et al.* (COHERENT Collaboration), First Detection of Coherent Elastic Neutrino-Nucleus Scattering on Argon, *Phys. Rev. Lett.* **126**, 012002 (2021).
 - [4] M. Cadeddu, C. Giunti, Y. F. Li, and Y. A. Y. Zhang, Average CsI Neutron Density Distribution from COHERENT Data, *Phys. Rev. Lett.* **120**, 072501 (2018).
 - [5] D. K. Papoulias, T. S. Kosmas, R. Sahu, V. K. B. Kota, and M. Hota, Constraining nuclear physics parameters with current and future COHERENT data, *Phys. Lett. B* **800**, 135133 (2020).
 - [6] R. Sahu, D. K. Papoulias, V. K. B. Kota, and T. S. Kosmas, Elastic and inelastic scattering of neutrinos and weakly interacting massive particles on nuclei, *Phys. Rev. C* **102**, 035501 (2020).
 - [7] O. Tomalak, P. Machado, V. Pandey, and R. Plestid, Flavor-dependent radiative corrections in coherent elastic neutrino-nucleus scattering, *J. High Energy Phys.* **02** (2021) 097.
 - [8] G. Co', M. Anguiano, and A. M. Lallena, Nuclear structure uncertainties in coherent elastic neutrino-nucleus scattering, *J. Cosmol. Astropart. Phys.* **04**, 044 (2020).
 - [9] D. K. Papoulias and T. S. Kosmas, COHERENT constraints to conventional and exotic neutrino physics, *Phys. Rev. D* **97**, 033003 (2018).
 - [10] D. K. Papoulias, T. S. Kosmas, and Y. Kuno, Recent probes of standard and non-standard neutrino physics with nuclei, *Front. Phys.* **7**, 191 (2019).
 - [11] Y. Efremenko (private communication).
 - [12] V. Tsakstara and T. S. Kosmas, Nuclear responses of ^{64}Zn and ^{66}Zn isotopes to supernova neutrinos, *Phys. Rev. C* **86**, 044618 (2012).
 - [13] H. Bonet, A. Bonhomme, C. Buck, K. Fulber, J. Hakenmuller, G. Heusser, T. Hugle, M. Lindner, W. Maneschg, T. Rink, H. Strecker, and R. Wink (CONUS Collaboration), Constraints on Elastic Neutrino Nucleus Scattering in the Fully Coherent Regime from the CONUS Experiment, *Phys. Rev. Lett.* **126**, 041804 (2021).
 - [14] V. Belov *et al.*, The νGeN experiment at the Kalinin Nuclear Power Plant, *JINST* **10**, P12011 (2015).
 - [15] V. Sharma, L. Singh, H. T. Wong, M. Agartioglu, J. W. Chen, M. Deniz, S. Kerman, H. B. Li, C. P. Liu, K. Saraswat, M. K. Singh, and V. Singh (TEXONO Collaboration), Studies of quantum-mechanical coherency effects in neutrino-nucleus elastic scattering, *Phys. Rev. D* **103**, 092002 (2021).
 - [16] D. Akimov *et al.* (COHERENT Collaboration), COHERENT 2018 at the spallation neutron source, [arXiv:1803.09183](https://arxiv.org/abs/1803.09183) [physics.ins-det].
 - [17] J. Billard *et al.*, Coherent neutrino scattering with low temperature bolometers at Chooz Reactor Complex, *J. Phys. G* **44**, 105101 (2017).
 - [18] G. Agnolet *et al.* (MINER Collaboration), Background studies for the MINER coherent neutrino scattering reactor experiment, *Nucl. Instrum. Meth. A* **853**, 53 (2017).
 - [19] G. Angloher *et al.* (NUCLEUS Collaboration), Exploring $CE\nu NS$ with NUCLEUS at the Chooz nuclear power plant, *Eur. Phys. J. C* **79**, 1018 (2019).
 - [20] A. Aguilar-Arevalo *et al.* (CONNIE Collaboration), Search for light mediators in the low-energy data of the CONNIE reactor neutrino experiment, *J. High Energy Phys.* **04** (2020) 054.

- [21] Coherent Captain Mills, <https://p25ext.lanl.gov/~lee/CaptainMills/>.
- [22] D. Baxter *et al.*, Coherent elastic neutrino-nucleus scattering at the European Spallation Source, *J. High Energy Phys.* **02** (2020) 123.
- [23] G. Fernandez-Moroni, P. A. N. Machado, I. Martinez-Soler, Y. F. Perez-Gonzalez, D. Rodrigues, and S. Rosauero-Alcaraz, The physics potential of a reactor neutrino experiment with Skipper CCDs: Measuring the weak mixing angle, *J. High Energy Phys.* **03** (2021) 186.
- [24] L. J. Flores *et al.* (SBC, CE ν NS Theory Group at IF-UNAM Collaboration), Physics reach of a low threshold scintillating argon bubble chamber in coherent elastic neutrino-nucleus scattering reactor experiments, *Phys. Rev. D* **103**, L091301 (2021).
- [25] A. Galindo-Uribarri, O. G. Miranda, and G. S. Garcia, A novel approach for the study of CE ν NS, [arXiv:2011.10230](https://arxiv.org/abs/2011.10230) [hep-ph].
- [26] A. Drukier and L. Stodolsky, Principles and applications of a neutral current detector for neutrino physics and astronomy, *Phys. Rev. D* **30**, 2295 (1984).
- [27] M. Lindner, W. Rodejohann, and X.-J. Xu, Coherent neutrino-nucleus scattering and new neutrino interactions, *J. High Energy Phys.* **03** (2017) 097.
- [28] P. Pirinen, J. Suhonen, and E. Ydrefors, Neutral-current neutrino-nucleus scattering off Xe isotopes, *Adv. High Energy Phys.* **2018**, 9163586 (2018).
- [29] V. Tsakstara and T. S. Kosmas, Low-energy neutral-current neutrino scattering on Te-128, Te-130 isotopes, *Phys. Rev. C* **83**, 054612 (2011).
- [30] V. Tsakstara and T. S. Kosmas, Analyzing astrophysical neutrino signals using realistic nuclear structure calculations and the convolution procedure, *Phys. Rev. C* **84**, 064620 (2011).
- [31] L. J. Flores, N. Nath, and E. Peinado, Non-standard neutrino interactions in $U(1)'$ model after COHERENT data, *J. High Energy Phys.* **06** (2020) 045.
- [32] D. Aristizabal Sierra, V. De Romeri, and N. Rojas, COHERENT analysis of neutrino generalized interactions, *Phys. Rev. D* **98**, 075018 (2018).
- [33] J. Liao and D. Marfatia, COHERENT constraints on nonstandard neutrino interactions, *Phys. Lett. B* **775**, 54 (2017).
- [34] C. Giunti, General COHERENT constraints on neutrino non-standard interactions, *Phys. Rev. D* **101**, 035039 (2020).
- [35] O. G. Miranda, D. K. Papoulias, G. Sanchez Garcia, O. Sanders, M. Tórtola, and J. W. F. Valle, Implications of the first detection of coherent elastic neutrino-nucleus scattering (CE ν NS) with liquid argon, *J. High Energy Phys.* **05** (2020) 130; **01** (2021) 067(E).
- [36] P. C. Srivastava, R. Sahu, and V. K. B. Kota, Shell model results for $T=1$ and $T=0$ bands in ^{66}As , *J. Phys. G* **44**, 125107 (2017).
- [37] T. S. Kosmas, A. Faessler, and R. Sahu, Transition matrix elements for μe conversion in Ge-72 using the deformed Hartree-Fock method, *Phys. Rev. C* **68**, 054315 (2003).
- [38] R. Sahu, P. C. Srivastava, and V. K. B. Kota, Deformed shell model results for neutrinoless positron double beta decay of nuclei in the $A = 60-90$ region, *J. Phys. G* **40**, 095107 (2013).
- [39] R. Sahu and V. K. B. Kota, Deformed shell model results for neutrinoless double beta decay of nuclei in $A = 60-90$ region, *Int. J. Mod. Phys. E* **24**, 1550022 (2015).
- [40] R. Sahu and V. K. B. Kota, Deformed shell model study of event rates for WIMP- ^{73}Ge scattering, *Mod. Phys. Lett. A* **32**, 1750210 (2017).
- [41] D. K. Papoulias, R. Sahu, T. S. Kosmas, V. K. B. Kota, and B. Nayak, Novel neutrino-floor and dark matter searches with deformed shell model calculations, *Adv. High Energy Phys.* **2018**, 6031362 (2018).
- [42] G. B. Gelmini, V. Takhistov, and S. J. Witte, Geoneutrinos in large direct detection experiments, *Phys. Rev. D* **99**, 093009 (2019).
- [43] N. Van Dessel, V. Pandey, H. Ray, and N. Jachowicz, Nuclear structure physics in coherent elastic neutrino-nucleus scattering, [arXiv:2007.03658](https://arxiv.org/abs/2007.03658) [nucl-th].
- [44] O. G. Miranda, D. K. Papoulias, O. Sanders, M. Tórtola, and J. W. F. Valle, Future CE ν NS experiments as probes of lepton unitarity and light-sterile neutrinos, *Phys. Rev. D* **102**, 113014 (2020).
- [45] T. S. Kosmas, D. K. Papoulias, M. Tortola, and J. W. F. Valle, Probing light sterile neutrino signatures at reactor and Spallation Neutron Source neutrino experiments, *Phys. Rev. D* **96**, 063013 (2017).
- [46] B. C. Cañas, E. A. Garcés, O. G. Miranda, and A. Parada, The reactor antineutrino anomaly and low energy threshold neutrino experiments, *Phys. Lett. B* **776**, 451 (2018).
- [47] H. T. Wong, H.-B. Li, J. Li, Q. Yue, and Z.-Y. Zhou, Research program towards observation of neutrino-nucleus coherent scattering, *J. Phys. Conf. Ser.* **39**, 266 (2006).
- [48] O. G. Miranda, D. K. Papoulias, M. Tórtola, and J. W. F. Valle, Probing neutrino transition magnetic moments with coherent elastic neutrino-nucleus scattering, *J. High Energy Phys.* **07** (2019) 103.
- [49] D. K. Papoulias, COHERENT constraints after the COHERENT-2020 quenching factor measurement, *Phys. Rev. D* **102**, 113004 (2020).
- [50] O. G. Miranda, D. K. Papoulias, M. Tórtola, and J. W. F. Valle, Probing new neutral gauge bosons with CE ν NS and neutrino-electron scattering, *Phys. Rev. D* **101**, 073005 (2020).
- [51] P. B. Denton and J. Gehrlein, A statistical analysis of the COHERENT data and applications to new physics, *J. High Energy Phys.* **04** (2021) 266.
- [52] M. Abdullah, J. B. Dent, B. Dutta, G. L. Kane, S. Liao, and L. E. Strigari, Coherent elastic neutrino nucleus scattering as a probe of a Z' through kinetic and mass mixing effects, *Phys. Rev. D* **98**, 015005 (2018).
- [53] B. Dutta, D. Kim, S. Liao, J.-C. Park, S. Shin, and L. E. Strigari, Dark Matter Signals from Timing Spectra at Neutrino Experiments, *Phys. Rev. Lett.* **124**, 121802 (2020).
- [54] L. M. G. de la Vega, L. J. Flores, N. Nath, and E. Peinado, Complementarity between dark matter direct searches and CE ν NS experiments in $U(1)'$ models, *J. High Energy Phys.* **09** (2021) 146.
- [55] K. S. Kumar, S. Mantry, W. J. Marciano, and P. A. Souder, Low energy measurements of the weak mixing angle, *Ann. Rev. Nucl. Part. Sci.* **63**, 237 (2013).
- [56] M. Wang, G. Audi, F. G. Kondev, W. Huang, S. Naimi, and X. Xu, The AME2016 atomic mass evaluation (II). tables, graphs, and references, *Chin. Phys. C* **41**, 030003 (2017).
- [57] W. C. Louis, Searches for muon-to-electron (anti) neutrino flavor change, *Prog. Part. Nucl. Phys.* **63**, 51 (2009).
- [58] G. Mention, M. Fechner, T. Lasserre, T. A. Mueller, D. Lhuillier, M. Cribier, and A. Letourneau, The reactor antineutrino anomaly, *Phys. Rev. D* **83**, 073006 (2011).

- [59] V. I. Kopeikin, L. A. Mikaelyan, and V. V. Sinev, Spectrum of electronic reactor anti-neutrinos, *Phys. Atom. Nucl.* **60**, 172 (1997) [*Yad. Fiz.* **60**, 230 (1997)].
- [60] Y. Huang, V. Chubakov, F. Mantovani, R. L. Rudnick, and W. F. McDonough, A reference earth model for the heat producing elements and associated geoneutrino flux, [arXiv:1301.0365](https://arxiv.org/abs/1301.0365) [physics.geo-ph].
- [61] L. Ludhova and S. Zavatarelli, Studying the Earth with geoneutrinos, *Adv. High Energy Phys.* **2013**, 425693 (2013).
- [62] C. A. J. O'Hare, Can we overcome the neutrino floor at high masses? *Phys. Rev. D* **102**, 063024 (2020).
- [63] V. K. B. Kota and R. Sahu, *Structure of Medium Mass Nuclei: Deformed Shell Model and Spin-Isospin Interacting Boson Model* (CRC Press, Boca Raton, FL, 2016).
- [64] H. Bonet *et al.*, Large-size sub-keV sensitive germanium detectors for the CONUS experiment, *Eur. Phys. J. C* **81**, 267 (2021).
- [65] B. Cheal, E. Mane, J. Billowes, M. L. Bissell, K. Blaum, B. A. Brown, F. C. Charlwood, K. T. Flanagan, D. H. Forest, C. Geppert, M. Honma, A. Jokinen, M. Kowalska, A. Krieger, J. Kramer, I. D. Moore, R. Neugart, G. Neyens, W. Nortershauser, M. Schug, H. H. Stroke, P. Vingerhoets, D. T. Yordanov, and M. Zakova, Nuclear Spins and Moments of Ga Isotopes Reveal Sudden Structural Changes Between $N = 40$ and $N = 50$, *Phys. Rev. Lett.* **104**, 252502 (2010).
- [66] D. P. Ahalpara, K. H. Bhatt, and R. Sahu, Collective bands in ^{81}Sr , *J. Phys. G* **11**, 735 (1985).
- [67] M. Honma, T. Otsuka, B. A. Brown, and T. Mizusaki, New effective interaction for pf shell nuclei and its implications for the stability of the $N = Z = 28$ closed core, *Phys. Rev. C* **69**, 034335 (2004).
- [68] B. A. Brown and W. A. Richter, New 'USD' Hamiltonians for the sd shell, *Phys. Rev. C* **74**, 034315 (2006).
- [69] A. Magilligan and B. A. Brown, New isospin-breaking "USD" Hamiltonians for the sd shell, *Phys. Rev. C* **101**, 064312 (2020).
- [70] T. Kosmas *et al.* (unpublished).
- [71] I. Angeli and K. Marinova, Table of experimental nuclear ground state charge radii: An update, *At. Data Nucl. Data Tables* **99**, 69 (2013).
- [72] B. Brown, R. Radhi, and B. Wildenthal, Electric quadrupole and hexadecupole nuclear excitations from the perspectives of electron scattering and modern shell-model theory, *Phys. Rep.* **101**, 313 (1983).
- [73] G. Mukherjee and S. K. Sharma, Inelastic electron scattering form factors for the excitation of $2+$ states in some $2p-1f$ shell nuclei, *Phys. Rev. C* **29**, 2101 (1984).
- [74] R. Agnese *et al.* (SuperCDMS Collaboration), Projected sensitivity of the SuperCDMS SNOLAB experiment, *Phys. Rev. D* **95**, 082002 (2017).
- [75] S. R. Klein and J. Nystrand, Exclusive vector meson production in relativistic heavy ion collisions, *Phys. Rev. C* **60**, 014903 (1999).
- [76] P. Coloma, P. B. Denton, M. C. Gonzalez-Garcia, M. Maltoni, and T. Schwetz, Curtailing the dark side in non-standard neutrino interactions, *J. High Energy Phys.* **04** (2017) 116.
- [77] D. Aristizabal Sierra, V. De Romeri, L. J. Flores, and D. K. Papoulias, Impact of COHERENT measurements, cross section uncertainties, and new interactions on the neutrino floor, [arXiv:2109.03247](https://arxiv.org/abs/2109.03247) [hep-ph].